JULY 1979 PPPL-1562
UC-20g

THEORY OF DRIFT-WAVE EIGENMODES IN TOROIDAL PLASMAS

BY

L. CHEN AND C. Z. CHENG

PLASMA PHYSICS LABORATORY

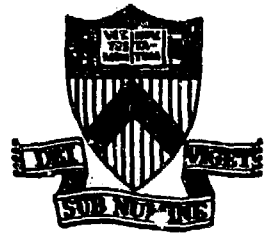

PRINCETON UNIVERSITY
PRINCETON, NEW JERSEY

This work was supported by the U. S. Department of Energy Contract No. EY-76-C-02-3073. Reproduction, translation, publication, use and disposal, in whole or in part, by or for the United States Government is permitted.

Theory of Drift-Wave Eigenmodes in Toroidal Plasmas

Liu Chen and C.Z. Cheng
Plasma Physics Laboratory, Princeton University
Princeton, New Jersey 08544

The eigenmode equation describing ballooning drift waves in toroidal plasmas is analyzed using the WKB method. Two branches of eigenmodes are identified. One is slab-like and the other is a new branch induced by the finite toroidicity. The slab-like eigenmodes correspond to unbounded states and experience finite shear damping. The toroidicity-induced eigenmodes, however, correspond to local quasibounded states with negligible shear damping. Both branches of eigenmodes may exist simultaneously. Corresponding analytical theories are also presented.

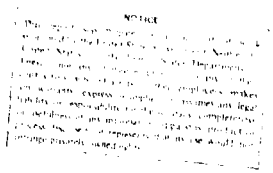

I. INTRODUCTION

Recently, there has been an active interest in the stability properties of drift-wave eigenmodes in sheared magnetic fields. A crucial point to realize in the stability analysis is, in the presence of finite magnetic shears, drift-wave eigenmodes in slab geometries experience anti-well potential structures and, therefore, finite damping due to energy convecting away from the mode-rational surface. The existence of this shear-induced convective damping or, simply, shear damping was first pointed out by Pearlstein and Berk.[1] Indeed, it is now well established that the shear damping is so effective that both the collisionless[2-5] and the collisional[6] "universal" drift-wave eigenmodes are stabilized in slab geometries. On the otherhand, as first emphasized by Taylor,[7] the shear damping mechanism may be modified significantly in toroidal plasmas, such as tokamaks. The physical arguments are as follows. In toroidal geometries, the mode-rational surfaces corresponding to different poloidal mode numbers are closely packed. Due to toroidal effects, such as curvature drifts, the neighboring poloidal modes are coupled. The drift-wave eigenmode centered about one particular mode-rational surface will be, therefore, affected by the wave energies which convect away from the neighboring eigenmodes. In other words, toroidal-coupling effects can modify the anti-well potential structure and, thereby, the shear damping mechanism.

In this work, we have employed the ballooning-mode formalism[7,8-10] and analyzed the effects of toroidal couplings on the shear damping of drift-wave eigenmodes. The toroidal-coupling effects considered here are those due to the usual ion ∇B and curvature drifts.[11-13]

The theoretical model and the corresponding drift-ballooning eigenmode equation are given in Sec. II. In Sec. III, we discuss the relevant boundary conditions. Applying these boundary conditions, the eigenmode equation is analyzed using the WKB method.[14,15] The results of WKB analyses are presented in Sec. IV. Based on the WKB results, we have developed corresponding analytical theories, which are described in Sec. V. Final conclusions and discussions are given in Sec. VI.

The WKB method employed here, when comparing with the usual numerical shooting schemes, has several advantages. (a) There is no difficulty in dealing with eigensolutions which are asymptotically divergent (see Sec. III). (b) Using the Stokes diagram, one can readily identify the various branches of eigenmodes and follow their evolutions as the parameters are changed. (c) With the Stokes diagram, the subdominant regions in the complex plane can be located. Numerical solutions can then be done in the complex plane to compare with the WKB results. In this respect, this work not only clarifies the results obtained elsewhere,[12,13] but also contains new findings as well as analytical theories.

II. THEORETICAL MODEL AND EIGENMODE EQUATION

Let us consider electrostatic drift waves in an axisymmetric, large-aspect-ratio torus with concentric, circular magnetic surface.[11] We adopt the usual (r,θ,ξ) coordinates corresponding, respectively, to the (minor) radial, poloidal and toroidal directions. The perturbed potential ϕ can be expressed as

$$\phi(r, \theta, \xi) = \sum_j \hat{\phi}_j(s) \exp [i(m_o\theta + j\theta - n\xi - \omega t)], \quad (1)$$

where $|j| << |m_o|$, $s = (r - r_o)/\Delta r_s$, r_o is the reference mode-rational surface $m_o = nq(r_o)$, $\Delta r_s = 1/k_\theta \hat{s}$, $k_\theta = m_o/r_o$ and $\hat{s} = rq'/q$ at $r = r_o$. Following standard procedures,[11] the two-dimensional eigenmode equation can be straightforwardly derived and is given by

$$[L(s, j) + Q_1(s, j) - \varepsilon_n T/\Omega]\hat{\phi}_j(s) = 0, \quad (2)$$

where

$$L = b_\theta (\hat{s}^2 d^2/ds^2 - 1), \quad (3)$$

$$Q_1 = 1/\Omega - 1 + [(s - j)/\eta_s\Omega]^2, \quad (4)$$

and $$T\hat{\phi}_j(s) = \hat{\phi}_{j+1}(s) + \hat{\phi}_{j-1}(s) + \hat{s}\frac{\partial}{\partial s}[\hat{\phi}_{j+1}(s) - \hat{\phi}_{j-1}(s)]. \quad (5)$$

Here, $b_\theta = k_\theta^2\rho_s^2$, $\rho_s = c_s/\omega_{ci}$, $c_s = (T_e/M_i)^{1/2}$, $\Omega = \omega/\omega_{*e}$, $\eta_s = qb_\theta^{1/2}/\varepsilon_n$, $\varepsilon_n = r_n/R$, $r_n^{-1} = |d\ln N/dr|$ and the remainder notations are standard. In deriving Eqs. (2)-(5), we have assumed $\tau = T_e/T_i >> 1$ and made the small ion-Larmor-radius as well as fluid-ion approximations. Furthermore, we have only kept the adiabatic electron response and ignored any electron destabilizing, temperature-gradient, or trapped-particle effects. We note that T, as defined in Eq. (5), is the toroidal-coupling operator due

to ion ∇B and curvature drifts. We remark that we have suppressed the destabilizing effects here in order to concentrate on the shear damping mechanism in toroidal plasmas. However, it needs to be emphasized that, (as stability analyses in slab geometries have clearly indicated,) modifications in the shear damping mechanism will have direct implications to the stability properties.

Since, typically, $|m_o| \sim |n| \sim |r_n/\rho_s| \sim O(10^2 - 10^3)$, we may adopt the large-n ballooning-mode formalism.[8-10] In the zeroth order, we have, with $z = s - j$, $\hat{\phi}_j(s) = \Phi(z)$ and $\hat{\phi}_{j \pm 1}(s) = \Phi(z \mp 1)$; i.e., the eigenmodes are composed of identical structures centered at each mode-rational surfaces. Equation (2) then reduces to a <u>one-dimensional</u> differential-difference equation; i.e.,

$$[L_1 + Q_1(z) - \epsilon_n T_1/\Omega]\Phi(z) = 0, \tag{6}$$

where $L_1 = b_\theta(\hat{s}^2 d^2/dz^2 - 1)$, $Q_1(z) = 1/\Omega - 1 + z^2/\Omega^2 n_s^2$, and

$$T_1\Phi = \Phi(z + 1) + \Phi(z - 1) + \hat{s}\,\frac{d}{dz}\,[\Phi(z - 1) - \Phi(z + 1)]. \tag{7}$$

Fourier transforming Eq. (6), we then obtain

$$[d^2/d\eta^2 + \eta_s^2\Omega^2 Q(\Omega,\eta)]\;\hat{\Phi}(\eta) = 0; \quad -\infty < \eta < \infty, \tag{8}$$

where

$$Q(\Omega,\eta) = b_\theta(1 + \hat{s}^2\eta^2) + 1 - 1/\Omega + (2\epsilon_n/\Omega)$$

$$(\cos\eta + \hat{s}\eta\sin\eta), \tag{9}$$

and η can be regarded as the coordinate along the field lines.[8-10] Equation (8) is the drift-ballooning eigenmode equation to be analyzed here. We note that Eq. (8) corresponds to perturbations centered at the outside of the torus and similar equations also have been derived by other authors.[12,13,16] Equation (9) shows that toroidal-coupling effects intrduce modulations on the otherwise anti-well potential structures. As mentioned earlier, we shall solve Eq. (8) using the WKB method. Before proceeding with the WKB analysis, however, we need to discuss the relevant boundary conditions.

III. BOUNDARY CONDITIONS

As $|\eta| \to \infty$, $Q \to b_\theta\hat{s}^2\eta^2$ and, for $\hat{\phi} = \exp\left[\pm i\int^\eta k_\eta d\eta\right]$,

we have

$$k_\eta \to \Omega\eta_s b_\theta^{1/2}\hat{s}\eta, \tag{10}$$

or

$$\hat{\phi} \to \exp\left[\pm i\Omega\eta_s b_\theta^{1/2}\hat{s}\eta^2/2\right). \tag{11}$$

For unstable eigenmodes (Im $\Omega > 0$), that $\hat{\phi}$ must be spatially decaying requires us to take the plus sign; i.e.,

$$\hat{\phi} \to \exp\ (i\Omega\eta_s b_\theta^{1/2}\hat{s}\eta^2/2). \tag{12}$$

Noting that

$$\partial\Omega/\partial k_{\parallel} \to (\eta_s b_\theta^{1/2}\hat{s}\eta)^{-1}, \tag{13}$$

the boundary condition, as given by Eq. (12), then corresponds to outward wave energy propagation. On the other hand, there is a difficulty in applying the outgoing-wave boundary condition, Eq. (12), to the marginally stable and damped eigenmodes (Im $\Omega \leq 0$); which will not asymptotically decay. This difficulty, however, can be readily resolved by noting that, in the original configuration (z) coordinate, the outgoing-wave boundary condition is equivalent to the asymptotically decaying condition if the linear ion Landau damping term is included.[1] One would, therefore, expect similar properties in the Fourier transformed η coordinate.[12]

Retaining the ion Landau damping term, it is easy to show that the potential structure, Q, is modified to be

$$\tilde{Q} = Q + i\tau\sqrt{\pi}\ \xi_i\ \exp\ (-\xi_i^2), \tag{14}$$

where ξ_i is an operator, $\xi_i = (\pi/2)^{1/2}\eta_s\Omega/|id/d\eta|$, and we have assumed $|\xi_i| > 1$, in deriving Eq. (14). Since $|\xi_i| > 1$, we may treat

the ion Landau damping term perturbatively. Thus, as $|\eta| \to \infty$, the WKB wave number becomes

$$k_\eta \to k_\eta \left[1 + i\tau \sqrt{\pi}\, \bar{\xi}_i \exp\left(-\bar{\xi}_i^2\right)/2b_\theta \hat{s}^2 \eta^2\right], \qquad (15)$$

where k_η is given by Eq. (10) and

$$\bar{\xi}_i = (\tau/2)^{1/2} \eta_s \Omega/|k_\eta| \to (\tau/2b_\theta)^{1/2}/\hat{s}|\eta|. \qquad (16)$$

Meanwhile, we have

$$\hat{\phi}(\eta) \to \exp\left(\pm i \int^\eta \tilde{k}_\eta d\eta\right). \qquad (17)$$

Since $\bar{\xi}_i > 0$, the requirement that the solutions decay asymptotically, again, leads us to take the plus sign, i.e., the outgoing-wave boundary condition; Eq. (12). Indeed, from Eqs. (15) and (16), we may view even in the η coordinate, that the boundary condition, Eq. (12), describes the wave energy being propagated outward and absorbed by the ion Landau damping at $|\eta| = \pm\infty$. Thus, Eq. (12) dictates that for damped eigenmodes (Im $\Omega < 0$) the solutions be asymptotically divergent. With the appropriate boundary conditions determined, the eigenvalue problem as posed by Eq. (8) is thus completely specified.

IV. RESULTS OF WKB ANALYSES

We present results of eigenmode analyses using the WKB (phase-integral) method. The WKB analyses are carried out with the interactive WKB code developed by White.[15] Detailed descriptions of this code are given in Ref. 15 and will not be repeated here.

In the present work, we have found that there exists two branches of eigenmodes. One is slab-like; i.e., this branch represents the continuation of the slab eigenmodes into the toroidal geometries. The corresponding Stokes diagram and potential structure along the real η axis, $-Q_r(\Omega, \eta_r)$, are shown in Fig. 1. We note that the complete Stokes structures are rather complicated and, therefore, only those anti-Stokes lines which are relevant in determining the eigenvalue condition are shown. As shown in Fig. 1(b), the potential structure is an anti-well; as in the slab limit. The wave energy, therefore, can freely convect outward and the eigenmodes are damped. The boundary condition, Eq. (12), thus dicates regions (i) and (i)' to be dominant and, hence, regions (ii) and (ii)' to be subdominant. The corresponding WKB eigenvalue condition is then

$$\Omega n_s \int_{-P}^{P} Q^{1/2} d\eta = (n + 1/2)\pi, \quad n = 0, 1, \ldots \tag{18}$$

The other branch of eigenmodes is induced by the finite toroidicity; i.e., it has no counterpart in the slab limit and, in this sense, is a new branch of eigenmodes. The details of

the eigenmodes, however, depend on the shear strength $\hat{s}$ and the toroidicity ε_n. Three cases have been identified: (a) $\hat{s} < 1/2$ and small ε_n, (b) $\hat{s} > 1/2$ and large ε_n, and (c) $\hat{s} < 1/2$. The corresponding Stokes diagrams and potential structures are given in Figs. 2, 3, and 4, respectively. According to the Stokes diagrams, we classify (a) as the weak toroidicity-induced eigenmodes; and (b) as well as (c) as strong toroidicity-induced eigenmodes. From Figs. 2-4 it is clear that these toroidicity-induced eigenmodes are characterized by eigenstates bounded by local potential wells, which may be localized either about or away from $\eta = 0$. Contrary to the slab-like branch with anti-well potentials, the outward convection of the wave energy occurs here only through the tunneling leakages. Therefore, we may expect the shear damping rates to be significantly reduced. In this respect, we may regard these eigenmodes to be quasi-bounded states which are quasi-marginally stable. Refering to Figs. 2 and 3 the WKB eigenvalue conditions for the weak and strong toroidicity-induced eigenmodes are, respectively,

$$\Omega n_s \int_{T_1}^{T_2} Q^{1/2} d\eta = (n + 1/2)\pi + \delta_1, \tag{19}$$

and

$$\Omega n_s \int_{-T_1}^{T_1} Q^{1/2} d\eta = (n + 1/2)\pi + \delta_2; \quad \text{for } n = 0, 1, \ldots \tag{20}$$

where δ_1 and δ_2 correspond to tunneling leakages and can be readily calculated. In general, the eigenvalue conditions, Eqs. (18)-(20), have to be solved numerically, and we may just as well apply the numerical shooting schemes in the complex plane. That is, with the Stokes diagrams given by the WKB results, we can locate the subdominant regions and, perform numerical shootings in a complex coordinate along which the solutions decay asymptotically. The results presented in this work are obtained by using this coupled WKB-numerical shooting scheme; which automatically includes the tunneling effects.

We have examined the evolution of the two branches of eigenmodes as the parameters, $\hat{s}$ and ε_n, are varied. Only the n = 0 eigenstate, which is least shear damped, is studied here. In the following results, we have fixed $b_\theta = 0.1$ and q = 1. Figures 5, 6, and 7 plot the eigenfrequencies, $\Omega = \Omega_r + i\Omega_i$, versus ε_n for $\hat{s} = 1$, 0.3 and 5, respectively. For comparision, the corresponding slab shear-damping rates are also shown. Figure 5 shows that, for $\hat{s} = 1$, only the slab-like branch exists for small ε_n, $\varepsilon_n \lesssim 0.075$. As $\varepsilon_n \gtrsim 0.075$, the weak toroidicity-induced branch appears, in addition, to the slab-like branch. As ε_n is further increased, the slab-like branch disappears for $\varepsilon_n > 0.1$ and the weak toroidicity-induced eigenmodes evolve into the strong toroidicity-induced eigenmodes. Regarding the shear damping rates, we note that the slab branch is further damped by the toroidicity. Meanwhile, for the toroidicity-induced branch, the shear damping rates are negligibly small; typically, $|\Omega_i| \sim O(10^{-3} - 10^{-4})$. In the weak shear ($\hat{s} = 0.3$),

case, Fig. 6 shows that the slab-like branch, which exists for $\varepsilon_n \geq 0.02$, is connected to the strong toroidicity-induced branch. Thus, in this case, there exists only a single branch of eigenmodes for a value of ε_n. Meanwhile, contrary to the $\hat{s} = 1$ case, the shear damping rates of the slab-like branch are somewhat reduced by the toroidicity. The toroidicity-induced branch, again, experiences negligible shear damping. The results of the strong shear ($\hat{s} = 5$) case, are shown in Fig. 7. While the general properties are similar to the $\hat{s} = 1$ case, there are two interesting differences. First, even with a strong shear, toroidicity-induced branch starts appearing at rather small ε_n. In fact, the critical value of ε_n, ε_{cT}, is about 0.05 which is less than the $\hat{s} = 1$ case; $\varepsilon_{cT} \simeq 0.075$. Second, the slab-like branch persists throughout the range of entire ε_n; i.e., up to $\varepsilon_n = 0.5$. Hence, both branches of eigenmodes exist for a wide range of ε_n. Figure 8 shows the dependence of the eigenmodes on the shear strength $\hat{s}$ for $\varepsilon_n = 0.1$. For small $\hat{s}$, $\hat{s} \lesssim 0.6$, only the strong toroidicity-induced eigenmodes exist; which evolve into the weak toroidicity-induced eigenmodes as $\hat{s}$ is increased. Meanwhile, the slab-like branch starts appearing at $\hat{s} \simeq 0.8$. Both branches then persist throughout the entire range of $\hat{s}$; up to $\hat{s} = 10$.

We now summarize the above results as follows:

(1) The slab-like branch exists when either, with $\hat{s}$ fixed $\varepsilon_n < \varepsilon_{cs}$, or, with ε_n fixed, $\hat{s} > \hat{s}_{cs}$.

(2) The slab-like branch has basically anti-well potential

structures and, therefore, experiences finite shear damping. Toroidicities further enhance (reduce) the shear damping rates for moderate and strong (weak) shear.

(3) The toroidicity-induced branch exists when $\epsilon_n > \epsilon_{cT}$ for a fixed $\hat{s}$ and persists into regimes with $\hat{s} \gg 1$.

(4) The toroidicity-induced branch corresponds to eigenstates quasi-bounded by local potential wells. Shear damping occurs through tunneling leakages and is, in general, negligibly small.

(5) Finally, for $\hat{s} \gtrsim 1$, both eigenmode branches may exist simultaneously.

The results described in this section provide useful insights in developing analytical theories: which not only, in turn, explain these results but also, more importantly, generalize the above results to a wider parameter space.

V. ANALYTICAL THEORIES

(A) Slab-Like Eigenmodes

For this branch of eigenmodes, the complex turning points are located near $\eta = 0$; i.e., $|P| < 1$ (c. f. Fig. 1). Therefore, we may assume $|\eta| < 1$ and approximate Q as

$$Q(\Omega,\eta) \simeq Q(\Omega,0) + Q''(\Omega,0)\eta^2/2, \tag{21}$$

where

$$Q(\Omega,0) = 1 + b_\theta - 1/\Omega + 2\epsilon_n/\Omega, \tag{22}$$

and

$$Q''(\Omega,0) = 2[b_0\hat{s}^2 + \epsilon_n(2\hat{s} - 1)/\Omega]. \tag{23}$$

Equation (8) then becomes a standard Weber's equation and can be readily solved. Applying the outgoing-wave boundary condition, we obtain the following dispersion relations

$$\Omega = \frac{1 - 2\epsilon_n}{1 + b_0} - i\,\frac{(2n+1)\epsilon_n}{q(1+b_0)}\left[\hat{s}^2 + \frac{\epsilon_n(2\hat{s}-1)}{b_\theta\Omega}\right]^{1/2}; \quad n = 0,1 \ldots \tag{24}$$

Since $\Omega_r > 0$, Eq. (24) clearly shows that for $\hat{s} > 1/2$ ($\hat{s} < 1/2$) the shear damping is further enchanced (reduced) by toroidal couplings. We note the assumption $|\eta| < 1$ is identical to Taylor's strong-coupling approximation.[7] Furthermore, while the eigenmodes are localized about $\eta = 0$ in the complex plane, they are extended along the η_r coordinate.

Since the slab-like branch requires that the potential structures be anti-well, it will cease to exist if either of the following two conditions occur

$$Q_r''(\Omega, 0) = 0, \tag{25}$$

and

$$Q_r(\Omega,\eta_o) = Q_r'(\Omega,\eta_o) = 0, \quad Q_r''(\Omega,\eta_o) > 0; \quad \text{at } \eta_o \neq 0. \tag{26}$$

In Eqs. (25) and (26), we have assumed $\Omega_r >> |\Omega_i|$, which is generally true. Equation (25) simply states that the anti-well potential structure about $\eta = 0$ is absent. Equation (26), on the other hand, indicates the appearance of well structure, which prohibits the wave energy from freely convecting outward.

For $\hat{s} < 1/2$, the relevant condition is Eq. (25); from which we obtain the cirtical value of ε_n, ε_{cs}, as

$$\varepsilon_{cs} = b_\theta \hat{s}^2/[(1 + b_\theta)(1 - 2\hat{s}) + 2b_\theta \hat{s}^2]. \qquad (27)$$

In Eq. (27), we have used the dispersion relation given by Eq. (24). For $b_\theta = 0.1$ and $\hat{s} = 0.3$, we find $\varepsilon_{cs} = 0.02$ in good agreement with the WKB result (c.f. Fig. 6).

For $\hat{s} > 1/2$, however, Eq. (25) never occurs and, Eq. (26) is the relevant condition. From $Q_r'(\Omega, \eta_o) = 0$, we have

$$b_\theta \hat{s}^2 \eta_o + (\varepsilon_{cs}/\Omega_r)[(\hat{s} - 1) \sin \eta_o + \hat{s}\eta_o \cos \eta_o] = 0. \qquad (28)$$

Assuming $|\eta_o| > 1$ and $b_\theta \hat{s} < \varepsilon_{cs}/\Omega_r$, Eq. (28) can be solved and we obtain

$$\eta_o \simeq 3\pi/2 - b_\theta \hat{s}\Omega_r/\varepsilon_{cs} + (\hat{s} - 1)2/3\pi\hat{s}. \qquad (29)$$

Using Eqs. (24) and (29) in the condition $Q_r(\Omega, \eta_o) = 0$ we obtain

$$\varepsilon_{cs} = \frac{b_\theta(\hat{s}^2\eta_o^2 - 1)}{2[1 + b_\theta\hat{s}^2\eta_o^2 + \hat{s}\eta_o(1 + b_\theta)]}, \tag{30}$$

and $\eta_o = 3\pi/2$. For $\hat{s} = 1$ and $b_\theta = 0.1$, we find $\varepsilon_{cs} \simeq 0.13$, which again, agrees well with the WKB result shown in Fig. 5. Finally, from Eqs. (24), (29), and (30), it can be easily shown that the assumptions η_o, $\varepsilon_{cs}/\Omega_r b_\theta \hat{s} > 1$ are justified.

(B) Toroidicity-Induced Eigenmodes

WKB results described in Sec. IV indicate that this eigenmode branch exists only for $\varepsilon_n \geq \varepsilon_{cT}$. For $\hat{s} < 1/2$, we have $\varepsilon_{cT} = \varepsilon_{cs}$ with ε_{cs} given by Eq. (27). In the following, we shall derive the analytical expression of ε_{cT} for $\hat{s} > 1/2$. At $\varepsilon_n = \varepsilon_{cT}$, the weak toroidicity-induced eigenmode branch appears and the corresponding potential structure, $-Q_r(\Omega,\eta_r)$, is shown in Fig. 9. From Fig. 9, we have the following five conditions

$$Q_r(\Omega,\eta_2) = 0, \tag{31}$$

$$Q_r'(\Omega,\eta_2) = 0, \tag{32}$$

$$Q_r'(\Omega,\eta_1) = 0, \tag{33}$$

$$Q_r(\Omega,\eta_3) = 0, \tag{34}$$

and

$$\int_{s_3}^{2} Q^{1/2}\, d\eta = (n + 1/2)\pi, \quad n = 0, 1, \ldots \qquad (35)$$

for the five unknowns; η_1, η_2, η_3, ε_{cT} and $\Omega = \Omega_{cT}$. Note in Eq. (35), we have neglected the tunneling leakage and, therefore, ε_{cT} is purely real. Since analytical expressions for Eq. (35) is generally difficult to obtain, we approximate the potential well about η_1 to be parabolic. Thus, in replacement of Eqs. (34) and (35), we have for the n = 0 eigenstate, the following condition

$$Q_r(\Omega_{cT}, \eta_1) = [-Q_r''(\Omega_{cT}, \eta_1)/b_\theta]^{1/2}(\varepsilon/q\Omega)_{cT}. \qquad (36)$$

To make further analytical progresses, we shall solve Eqs. (31), (32), (33), and (36) by successive approximations. That is, we assume η_1 and η_2 are sufficiently close to η_o, where $Q_r''(\eta_o) = 0$. We thus, let $\eta_1 = \eta_o - \delta_1$ and $\eta_2 = \eta_o + \delta_2$ with δ_1, $\delta_2 < 1$. Correspondingly, we let $\varepsilon_{cT} = \varepsilon_o + \varepsilon_1$ and $\Omega_{cT} = \Omega_o + \Omega_1$; such that $|\varepsilon_1/\varepsilon_o|$, $|\Omega_1/\Omega_o| < 1$. We then have $Q_r = Q_o + Q_1$, where

$$Q_o = 1 + b_\theta(1 + \hat{s}^2\eta^2) - 1/\Omega_o + (2\varepsilon/\Omega)_o(\cos\eta + \hat{s}\,\eta\sin\eta), \qquad (37)$$

and

$$Q_1 = \Omega_1/\Omega_0 + 2(\varepsilon/\Omega)_0\beta^2(\cos\eta + \hat{s}\,\eta\sin\eta), \tag{38}$$

with

$$\beta^2 = \varepsilon_1/\varepsilon_0 - \Omega_1/\Omega_0. \tag{39}$$

In the zeroth order, we have

$$Q_0(\Omega_0,\eta_0) \equiv \bar{Q}_0 = 0, \tag{40}$$

$$\bar{Q}_0' = 2\{b_\theta\hat{s}^2\eta_0 + (\varepsilon/\Omega)_0[(\hat{s} - 1)\sin\eta_0 + \hat{s}\eta_0\cos\eta_0]\} = 0, \tag{41}$$

and

$$Q_0'' = 2\{b_\theta\hat{s}^2 + (\varepsilon/\Omega)_0[(2\hat{s} - 1)\cos\eta_0 - \hat{s}\eta_0\sin\eta_0]\} = 0. \tag{42}$$

Equations (40)-(42) can be readily solved by assuming $|b_\theta\hat{s}^2 + (\varepsilon/\Omega)_0(2\hat{s} - 1)\cos\eta_0| < |(\varepsilon/\Omega)_0\hat{s}\eta_0|$. From Eq. (42), we obtain

$$\eta_0 = \pi - \delta_0, \tag{43}$$

and

$$\delta_0 = (b_\theta\hat{s}^2\Omega_0/\varepsilon_0 + 1 - 2\hat{s})/\hat{s}\pi. \tag{44}$$

From Eqs. (41), (43), and (44), we have

$$\varepsilon_0 \sim \varepsilon_0/b_\theta \hat{s}, \tag{45}$$

and

$$\delta_0 = (1 - \hat{s})/\hat{s}\pi. \tag{46}$$

In deriving Eqs. (45) and (46), we have ignored terms of $O(\delta_0/\pi) \sim O(\pi^{-2})$. Finally, from Eq. (40) we obtain

$$\varepsilon_0 = b_\theta \hat{s}/[1 + b_\theta(1 + \hat{s}^2\pi^2 - 2\hat{s}^2)]. \tag{47}$$

We now consider the corrections up to $O(\delta^2)$ with $\delta_1 \sim \delta_2 \sim \delta \sim \beta$. From Eqs. (32) and (34), we have $\delta_1 = \delta_2 \equiv \delta$ and

$$\delta^2 = -2Q_1'(\eta_0)/\bar{Q}_0^m, \tag{48}$$

where

$$Q_1'(\eta_0) \equiv \bar{Q}_1' = \beta^2 2b_\theta \hat{s}^2\pi, \tag{49}$$

$$\bar{Q}_0^m = -2b_\theta \hat{s}^2\pi a_1, \tag{50}$$

and

$$a_1 = 1 + (\hat{s} - 1)(4\hat{s} - 1)/\hat{s}^2\pi^2. \tag{51}$$

We note that we have used Eqs. (41), (42), and (45) in deriving Eqs. (49) and (50). Substituting Eqs. (49) and (50) into Eq. (48), we then have

$$\delta = b_1 \beta, \tag{52}$$

with

$$b_1 = (2/a_1)^{1/2}. \tag{53}$$

From Eq. (31), we have

$$\bar{Q}_1 + \delta \bar{Q}_1' = 0, \tag{54}$$

where $\bar{Q}_1'$ is given by Eq. (49) and $\bar{Q}_1$, Eq. (38) can be reduced to

$$\bar{Q}_1 = \Omega_1/\Omega_o^2 - 2b_\theta \hat{s}^2 \beta^2. \tag{55}$$

Equation (54) then becomes

$$\Omega_1/\Omega_o^2 - 2b_\theta \hat{s}^2 \beta^2 (1 + \delta\pi) = 0. \tag{56}$$

Meanwhile, Eq. (36) becomes

$$\bar{Q}_1 - \delta \bar{Q}_1' = [-(\bar{Q}_1'' - \delta \bar{Q}_o''')/b_\theta]^{1/2} (\varepsilon/q\Omega)_o. \tag{57}$$

Noting Eqs. (50), (52) and that

$$\bar{Q}_1'' = 2b_\theta \hat{s}^2 \beta^2, \tag{58}$$

we then have $|\bar{Q}_1''/\delta\bar{Q}_0'''| = \beta/\pi a_1 b_1 \ll 1$ and therefore, Eq. (57) becomes

$$\Omega_1/\Omega_0^2 - 2b_\theta \hat{s}^2\beta^2(1 - \delta\pi) = [2\pi a_1 b_1 \beta]^{1/2} b_\theta \hat{s}^2/q. \qquad (59)$$

Combining Eqs. (56) and (59) and noting $\delta = b_1\beta$, we obtain

$$\beta = (a_1/8\pi q^2 b_1)^{1/5}, \qquad (60)$$

and

$$\Omega_1/\Omega_0 = 2\hat{s}\beta^2(1 + \pi b_1\beta)\varepsilon_0. \qquad (61)$$

Equation (61) into Eq. (39) we then find

$$\varepsilon_1/\varepsilon_0 = \beta^2[1 + 2\hat{s}(1 + \pi b_1\beta)\varepsilon_0]. \qquad (62)$$

An interesting property predicted by the above analytical theory is, as either $b_\theta \to \infty$ or $\hat{s} \to \infty$, we have

$$\varepsilon_0 \to 1/\hat{s}(\pi^2 - 2 + \hat{s}^{-2}) \equiv d_0/\hat{s}, \qquad (63)$$

and

$$\varepsilon_{cT} \to (1 + d_1)d_0/\hat{s} \equiv \bar{\varepsilon}_c, \qquad (64)$$

where $d_1 = \hat{s}^2[1 + 2(1 + \cdots b_1\hat{s})d_0]$. That is, there exists a maximum value of $\hat{\epsilon}_{cT}$, $\bar{\epsilon}_c$, which is a constant for a fixed $\hat{s}$ and, as $\hat{s} \to \infty$, is inversely proportional to $\hat{s}$. This predicted property is consistent with the WKB results that the toroidicity-induced branch persists for $\hat{s} \to 1$.

For $q = s = 1$, we have plotted in Fig. 10 the analytically predicted $\hat{\epsilon}_{cT} = \hat{\epsilon}_0 + \hat{\epsilon}_1$ versus b_0. As can be seen, the analytical predictions agree rather well with the WKB results. Meanwhile, in this case, we find $\bar{\epsilon}_c \simeq 0.14$.

VI CONCLUSIONS AND DISCUSSIONS

In this work, we have examined the shear damping of drift-wave eigenmodes in toroidal plasmas. The toroidal-coupling effects considered here are due to the ion ∇B and curvature drifts. The corresponding drift-ballooning eigenmode equation, derived via the ballooning mode formalism, is then analyzed using the WKB method. It is found that toroidal couplings introduce modulations to the potential structures. Two eigenmode branches are then found to exist. One is slab-like and the other is a new branch induced by the finite toroidicity. The slab-like eigenmode branch exists for small toroidicities and has anti-well potential structures. The eigenmodes, thus, correspond to unbounded states and experience finite shear damping. For $\hat{s} = rq'/q > 1/2$, toroidal couplings further enhance the shear damping rates. For $\hat{s} < 1/2$, however, the shear damping rates are somewhat reduced by the toroidal effects. On the otherhand, the toroidicity-induced

eigenmode branch, which has no counterpart in the slab limit, is characterized by potential structures with local wells. For this branch, the eigenmodes correspond to eigenstates quasi-bounded by those local potential wells. Shear damping occurs only through tunneling leakages and is, generally, negligible. The toroidicity-induced eigenmodes, therefore, can be regarded as quasi-marginally stable. For certain parameters, both eigenmode branches can exist simultaneously. We have also developed corresponding analytical theories, which agree both qualitatively and quantatively with the WKB results. An interesting property predicted by the analytical theories is that the toroidicity-induced branch can exist even when b_θ, $\hat{s} \gg 1$ for reasonable toroidicities; i.e., $\varepsilon_n \sim O(10^{-1})$.

Since destablizing effects; such as electron dissipations, are suppressed here in order to concentrate on the shear damping effects, this work, therefore, does not answer the stability question. However, some remarks may be made on the implications of the present results to the stability properties. Let us concentrate on the universal drift mode. In this case, electron dissipations can be easily incorporated into the 1-D differential-difference eigenmode equation, Eq. (6). As noted in Sec. V, we may apply Taylor's strong-coupling approximation[7] for the slab-like branch. Equation (6) can then be reduced to a second-order differential equation and readily solved.[6,11,17] Generally speaking, the results show that unstable eigenmodes exist only for weak shears; i.e., $\hat{s} < 1/2$. As for the toroidicity-induced

eigenmode branch, since the eigenmodes are quasi-marginally stable, it may be expected that finite electron dissipations can render the eigenmodes to be absolutely unstable. This expectation, however, remains to be verified.

The existence of the toroidicity-induced eigenmode branch clearly indicates that, contrary to conventional thinkings, toroidal-coupling effects can not be simply regarded as (regular) perturbations to the slab eigenmode branch. In this respect, it is interesting to note the possibility that trapped particles can play not only the usual destabilizing role but also, through the associated toroidal-coupling effects, the new role of introducing new eigenmode branches.

Finally, we remark that the present analyses can be easily extended to consider perturbations which may be centered away from the outside of the torus.

ACKNOWLEDGMENTS

The authors acknowledge useful discussions with R. L. Dewar, E. A. Frieman, A. H. Glasser, and R. B. White.

This work was supported by the United States Department of Energy Contract No. EY-76-C-02-3073.

REFERENCES

[1] J. D. Pearlstein and H. L. Berk, Phys. Rev. Lett 23, 220 (1969).

[2] D. W. Ross and S. M. Mahajan, Phys. Rev. Lett. 40, 324 (1978). Also, K. T. Tsang, P. J. Catto, J. C. Whitson, and J. Smith, Phys. Rev. Lett. 40, 327 (1978).

[3] Liu Chen, P. N. Guzdar, R. B. White, P. K. Kaw, and C. Oberman, Phys. Rev. Lett. 41, 649 (1978).

[4] T. M. Antonsen, Jr., Phys. Rev. Lett. 41, 33 (1978).

[5] Y. C. Lee and Liu Chen, Phys. Rev. Lett. 42, 708 (1979).

[6] Liu Chen, P. N. Guzdar, J. Y. Hsu, P. K. Kaw, C. Oberman, and R. B. White, Nucl. Fusion 19, 373 (1979). Also, P. N. Guzdar, Liu Chen, P. K. Kaw, and C. Oberman, Phys. Rev. Lett. 40, 1566 (1978).

[7] J. B. Taylor, in Plasma Physics and Controlled Nuclear Fusion Research (Proc. 6th Int. Conf. Berchtesgaden, 1969) Vol. 2, (IAEA, Vienna, 1977), p.323.

[8] J. W. Connor, R. J. Hastie, and J. B. Taylor, Culham Laboratory Report CLM-P537 (1978), to be published.

[9] A. H. Glasser, M. S. Chance, R. L. Dewar, E. A. Frieman, J. M. Greene, R. C. Grimm, S. C. Jardin, J. L. Johnson, J. Manickam, M. Okabayashi, and A. M. M. Todd, Princeton Plasma Physics Laboratory Report PPPL-1468 (1978). Also R. L. Dewar, M. S. Chance, and A. H. Glasser, Proc. Sherwood Theory Meeting on Controlled Thermonuclear Fusion, Mont Pocono, PA, April 1979.

[10]Y. C. Lee and J. W. Van Dam, University of California at Los Angeles Report PPG-337 (1978).

[11]See, for example, W. M. Tang, Nucl. Fusion 18, 1089 (1978).

[12]R. J. Hastie, K. W. Hesketh, and J. B. Taylor, Culham Laboratory Report CLM-P575 (1979).

[13]D. I. Choi, W. Horton, and R. Estes, University of Texas at Austin Report FRCR-184 (1978).

[14]J. Heading, An Introduction to Phase Integral Methods (John Wiley, New York, 1962).

[15]R. B. White, J. Comput. Phys. 31, No. 3 (1979), to be published.

[16]E. A. Frieman, W. M. Tang, G. Rewoldt, and A. H. Glasser, Bull. Am. Phys. Soc. 23, 785 (1978).

[17]W. Horton, Jr., R. D. Estes, H. Kawk, and D. I. Choi, Phys. Fluids 21, 1366 (1978).

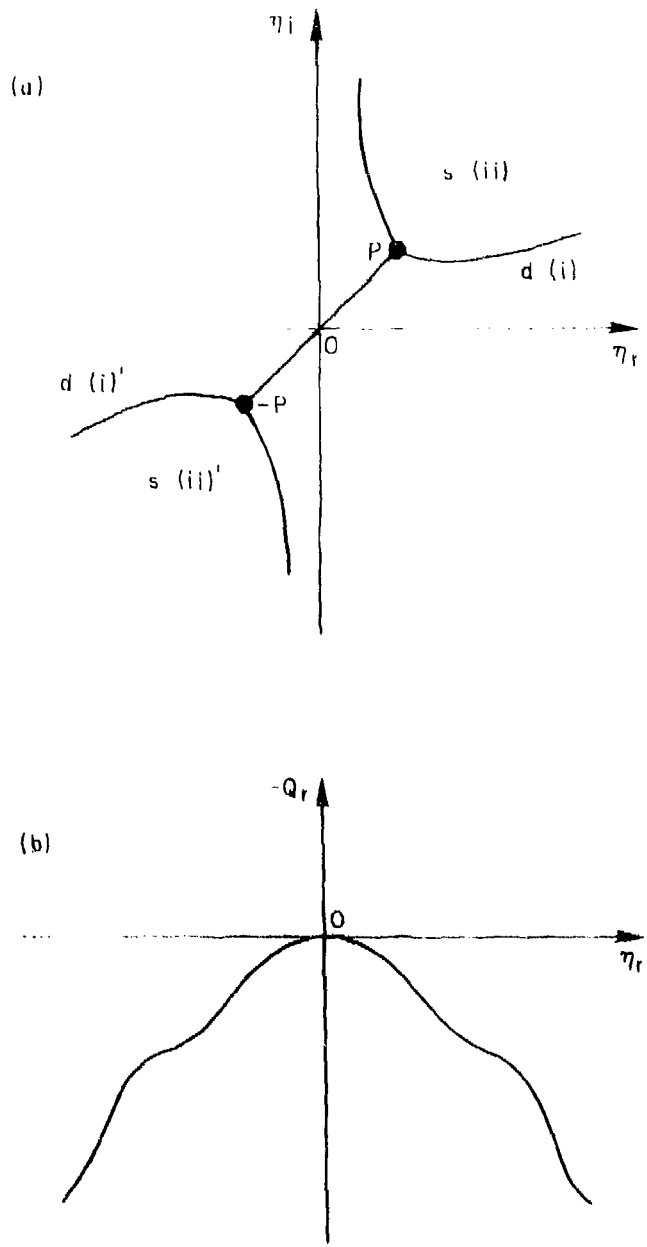

792269

Fig. 1. Typical (a) anti-Stokes plot and (b) potential structure for the slab-like eigenmode branch.

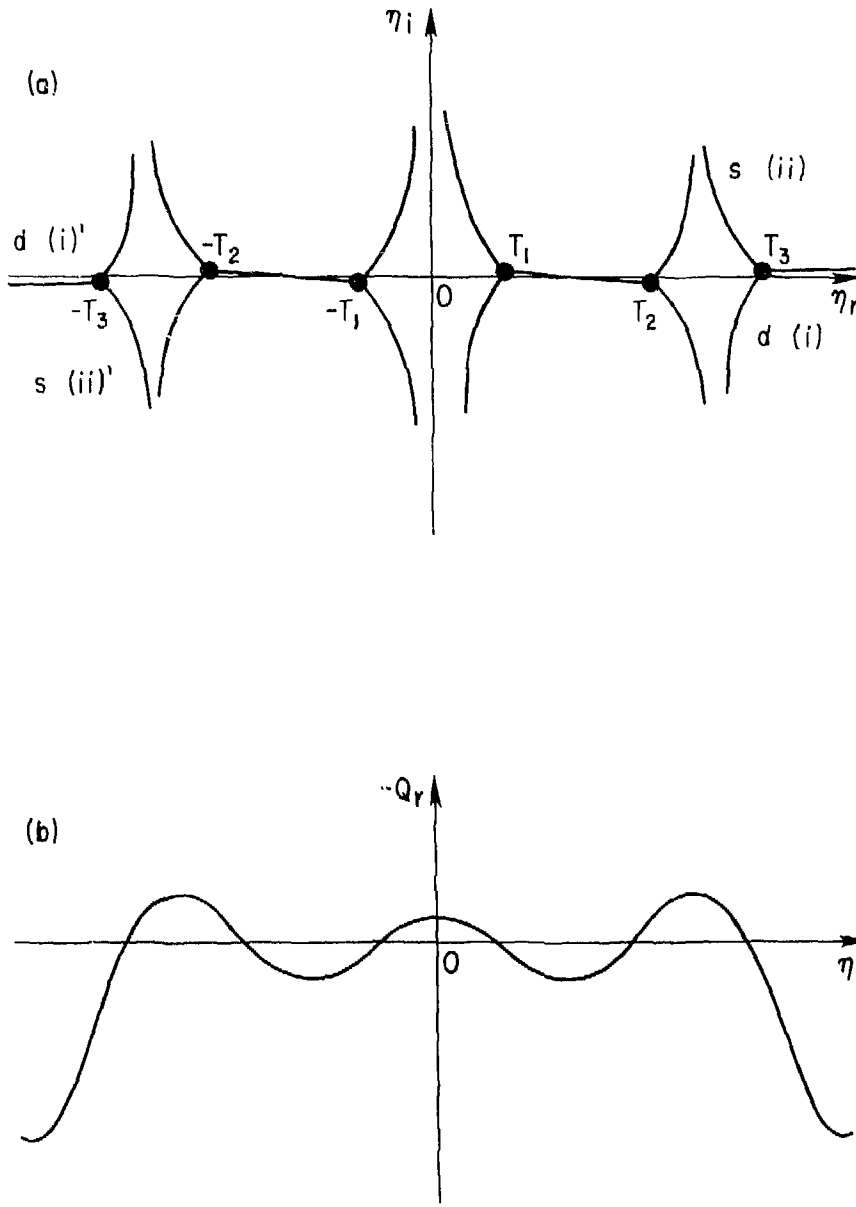

792268

Fig. 2. Typical (a) anti-Stokes plot and (b) potential structure for the weak toroidicity-induced eigenmode branch.

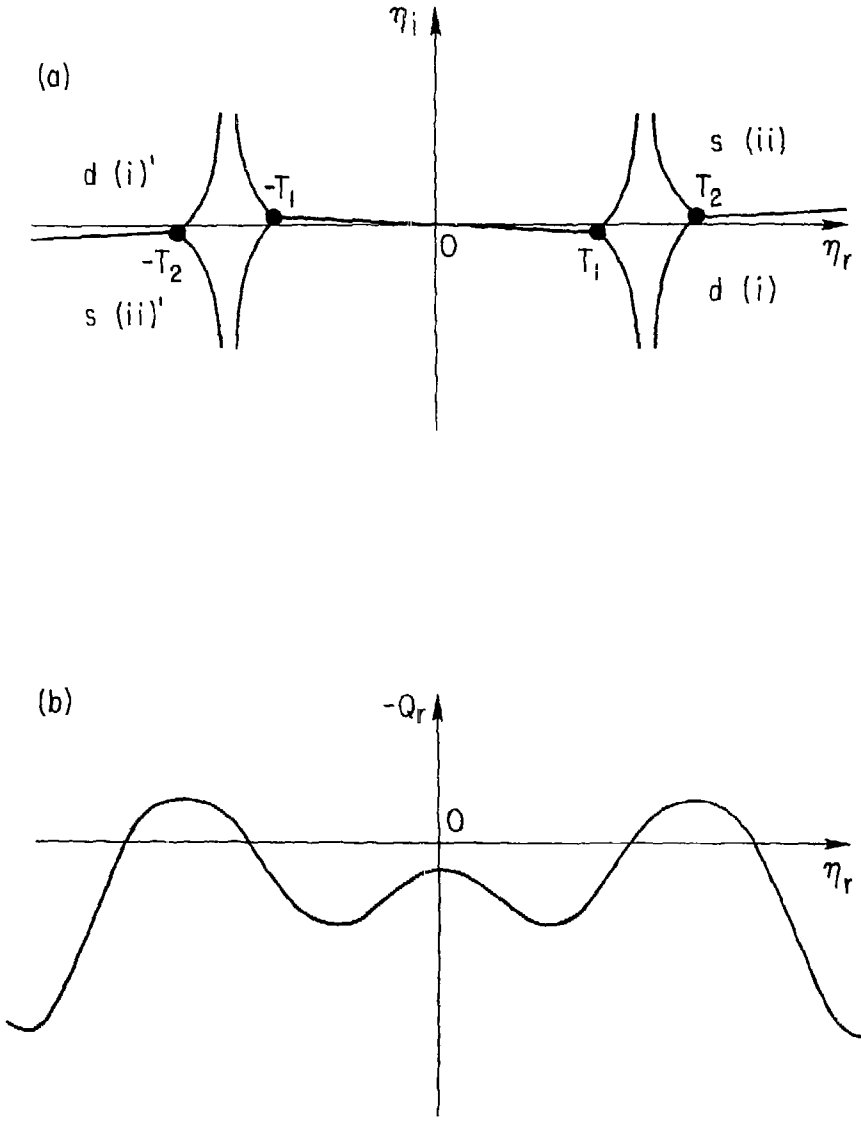

792270

Fig. 3. Typical (a) anti-Stokes plot and (b) potential structure for the strong toroidicity-induced eigenmode branch with $\hat{s} = rq'/q > 1/2$.

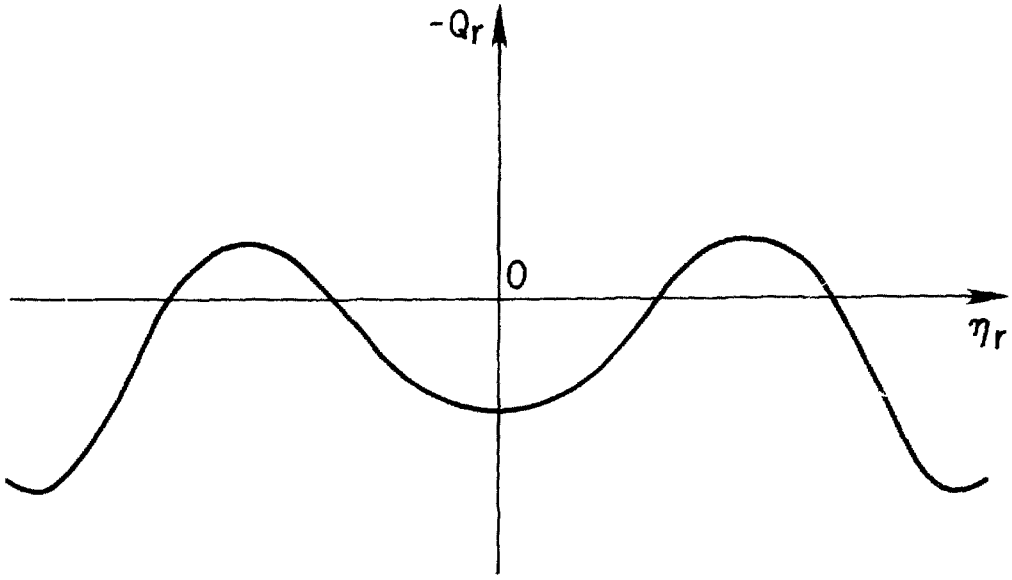

792266

Fig. 4. Typical potential structure for the strong toroidicity-induced eigenmode branch with $\hat{s} < 1/2$. The anti-Stokes plot is similar to Fig. 3(a).

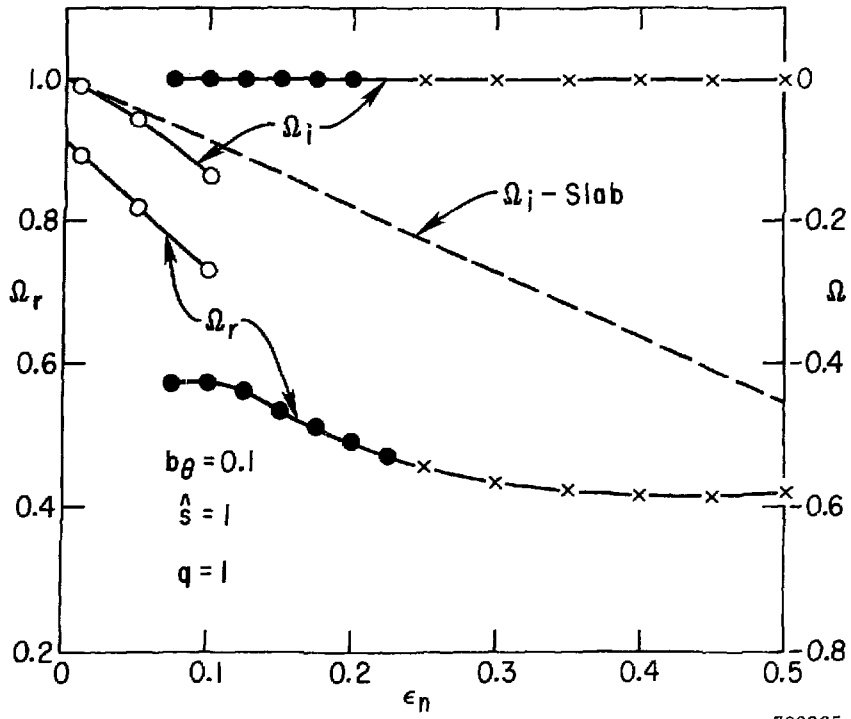

Fig. 5. Plot of eigenmode frequencies Ω versus ϵ_n for $b_\theta = 0.1$, $q = 1$, and $\hat{s} = 1.0$, • and x correspond, respectivly, to the slab-like, weak and strong toroidicity-induced eigenmodes.

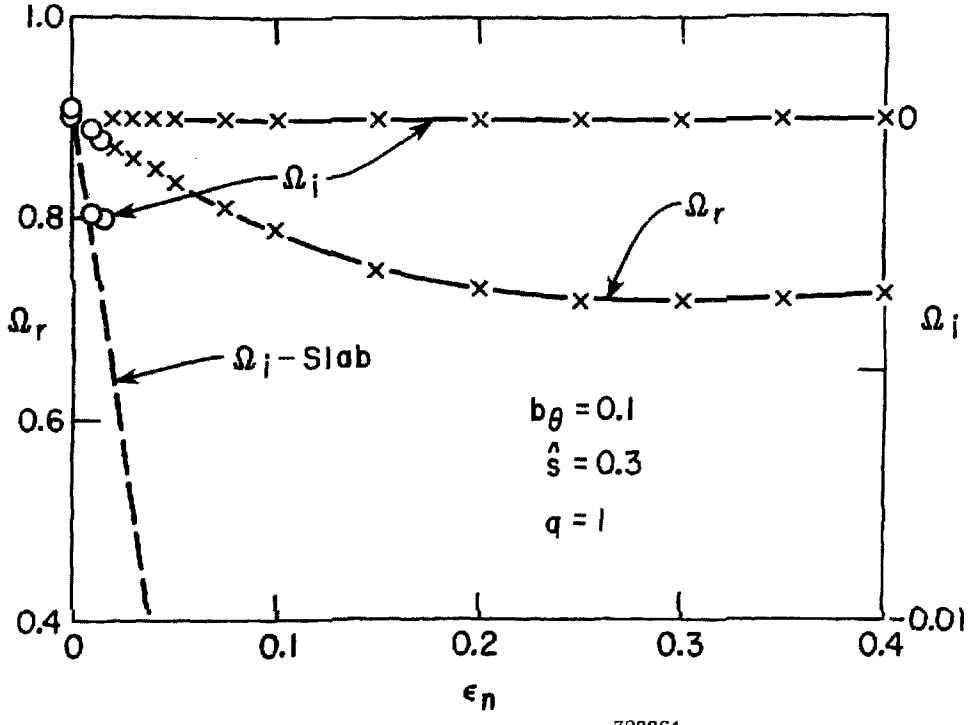

792264

Fig. 6. Same as Fig. 5, except $\hat{s} = 0.3$.

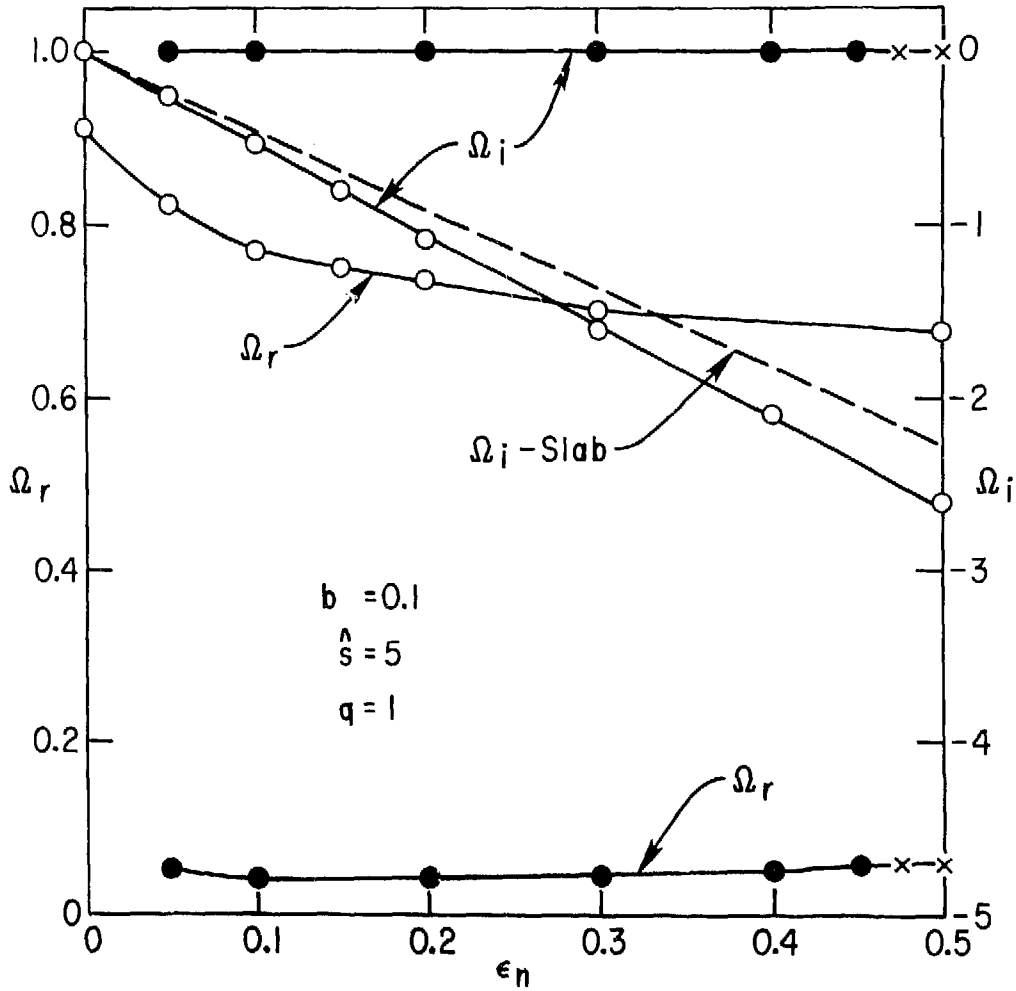

792271

Fig. . Same as Fig. 5, except $\hat{s}$ = 5.

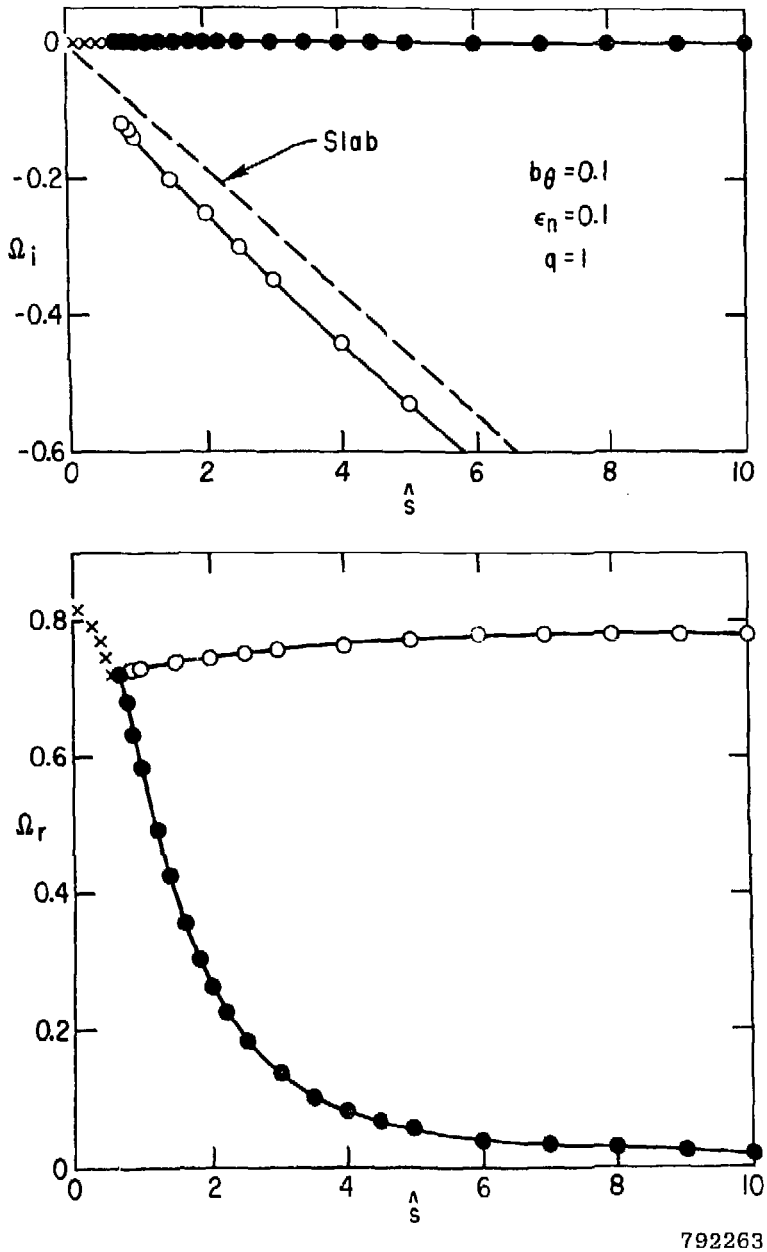

Fig. 8. Plot of Ω versus $\hat{s}$ for $b_\theta = 0.1$, $q = 1$, and $\epsilon_n = 0.1$. The rest is same as Fig. 5.

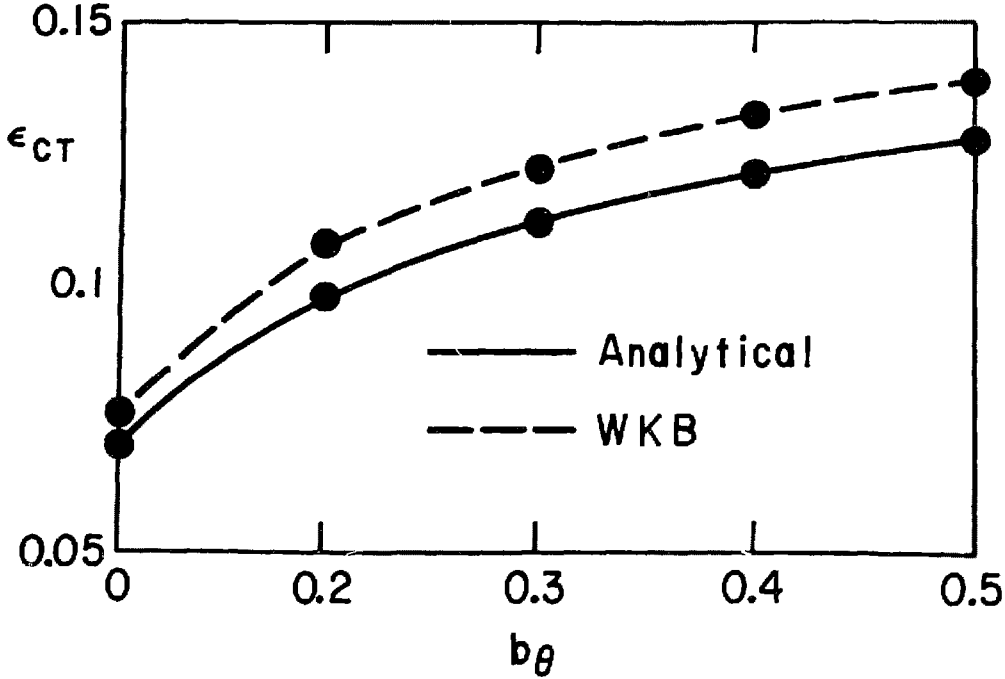

Fig. 9. Potential structure for $\varepsilon_n = \varepsilon_{cT}$, where the weak toroidicity-induced eigenmode branch appears.

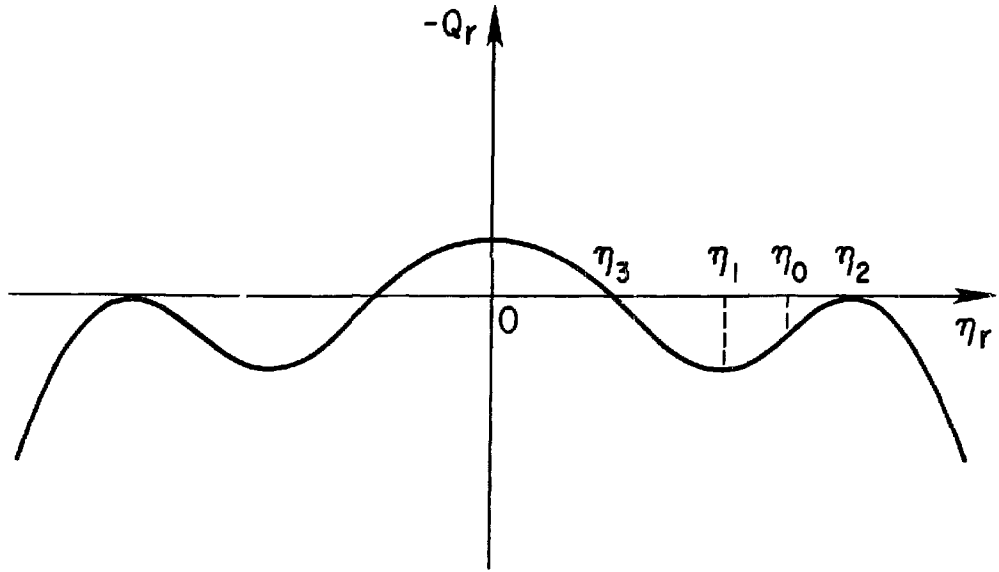

Fig. 10. Plots of ε_{cT} versus b_θ for $\varepsilon_n = 0.1$, $\hat{s} = 1$, and $q = 1$.

792267